water

MDPI

Article

Green Synthesis and Characterizations of Cobalt Oxide Nanoparticles and Their Coherent Photocatalytic and Antibacterial Investigations

Parvathiraja Chelliah [1,*], Saikh Mohammad Wabaidur [2], Hari Prapan Sharma [3], Muhsin J. Jweeg [4], Hasan Sh. Majdi [5], Munthir Mohammed Radhy AL. Kubaisy [6], Amjad Iqbal [7] and Wen-Cheng Lai [8,9,*]

1 Department of Physics, Manonmaniam Sundaranar University, Tirunelveli 627012, Tamilnadu, India
2 Department of Chemistry, College of Science, King Saud University, P.O. Box-2455, Riyadh 11451, Saudi Arabia
3 Department of Business Management, GLA University, Mathura 281406, Uttar Pradesh, India
4 College of Technical Engineering, Al-Farahidi University, Baghdad 10070, Iraq
5 Department of Chemical Engineering and Petroleum Industries, Al-Mustaqbal University College, Babylon 51001, Iraq
6 Department of Medical Physics, The University of Mashreq, Baghdad 10001, Iraq
7 Department of Materials Technologies, Silesian University of Technology, 44-100 Gliwice, Poland
8 Bachelor Program in Industrial Projects, National Yunlin University of Science and Technology, Douliu 640301, Taiwan
9 Department of Electronic Engineering, National Yunlin University of Science and Technology, Douliu 640301, Taiwan
* Correspondence: cpraja1206@gmail.com (P.C.); wenlai@yuntech.edu.tw or wenlai@mail.ntust.edu.tw (W.-C.L.)

Abstract: Water pollution is a serious concern for developing and undeveloped countries. Photocatalytic degradation of organic pollutants is an effective degradation method to restrain the green ecosystem. This research article presents a green, low-cost, and benevolent eco-friendly biosynthesis of cobalt oxide (Co_3O_4) nanoparticles using *Curcuma longa* plant extract. The UV and visible region absorbance of Co_3O_4 nanoparticles estimated the Co^{2+} and Co^{3+} transitions on the lattice oxygen, and their bandgap of 2.2 eV was confirmed from the UV-DRS spectroscopy. The cubic structure and spherical shape of Co_3O_4 nanoparticles were estimated by using XRD and TEM characterizations. Plant molecules aggregation and their agglomerations on the nanoparticles were established from FTIR and EDX spectroscopy. Multiple cobalt valences on the oxygen surfaces and their reaction, bonding, and binding energies were analyzed from XPS measurements. The biogenic Co_3O_4 nanoparticles were executed against gram-positive (*Staphylococcus aureus*—*S. aureus*) and gram-negative (*Escherichia coli*—*E. coli*) bacteria. A gram-positive bacterial strain exhibited great resistivity on Co_3O_4 nanoparticles. Degradation of organic dye pollutants on the Co_3O_4 nanoparticles was performed against methylene blue (MB) dye under the conditions of visible light irradiation. Dye degradation efficiency pseudo-first-order kinetics on the pseudo-first-order kinetics denotes the rate of degradation over the MB dye. This research work achieved enhanced degradation potency against toxic organic dye and their radicals are excited from visible light irradiations. Absorption light and charged particle recombinations are reformed and provoked by the plant extract bio-molecules. In this process, there is no inferior yield development, and electrons are robustly stimulated. Furthermore, the biosynthesized Co_3O_4 nanoparticles determined the potency of bacterial susceptibility and catalytic efficacy over the industrial dye pollutants.

Keywords: nanoparticles; photocatalysis; green synthesis; metal oxides; zero-valent atoms

check for updates

Citation: Chelliah, P.; Wabaidur, S.M.; Sharma, H.P.; Jweeg, M.J.; Majdi, H.S.; AL. Kubaisy, M.M.R.; Iqbal, A.; Lai, W.-C. Green Synthesis and Characterizations of Cobalt Oxide Nanoparticles and Their Coherent Photocatalytic and Antibacterial Investigations. *Water* **2023**, *15*, 910. https://doi.org/10.3390/w15050910

Academic Editor: Andreas Angelakis

Received: 16 January 2023
Revised: 23 February 2023
Accepted: 24 February 2023
Published: 27 February 2023

Copyright: © 2023 by the authors. Licensee MDPI, Basel, Switzerland. This article is an open access article distributed under the terms and conditions of the Creative Commons Attribution (CC BY) license (https://creativecommons.org/licenses/by/4.0/).

1. Introduction

Water contamination is currently a serious environmental problem and a major menace to community physical conditions all over the human race as a consequence of the speedy

advancement of economies, manufacturers, and population growth [1,2]. Most pollutant types include pesticides, dyes, pigments, phenol, organic contaminants, fungicides, e-waste, oil refineries, and so on [2,3]. When compared to other types of water pollutants, organic dyes are one of the most significant sources of environmental pollution [4,5]. Dye-based products attract a large portion of fast-moving consumer goods to humans because they are extensively used as color tones in the textile, printing, rubber, cosmetics, plastics, and leather industries [2–6]. The presence of hazardous materials in industrial wastewater endangers human health and aquatic organisms in the environment. Dyes are categorized into three major types: anionic, cationic, and non-ionic. These dyes are very stable and can only be decomposed at temperatures above 200 °C [3–6]. The presence of hazardous dye materials in industrial wastewater endangers human health and aquatic organisms in the environment [4–6]. Among them, cationic dyes are more colorful but have some toxic properties for humans, the environment, and ecology [5,6]. Methylene blue is a common cationic dye that is commonly applied in textiles, cosmetics, leather industries, paper industries, and foodstuffs [5,6]. After implanting, these dyes into their applied goods inappropriate releases of this dye contaminant into the water bodies create a major problem. It has been linked to several health risks, such as eye irritation, respiratory problems, gastrointestinal tract problems, and cerebral failure [6].

The elimination of the MB dye molecule from industrial effluent has been studied using a variety of methods, including enzymatic processes, photodegradation, chemical coagulation, electrochemical removal, ozonation, ion exchange, sonication, membrane filtration, and physical adsorption [7–9]. Among these commercial methods, photocatalysis is gaining popularity due to its simple process, easy catalytic recovery, and low secondary pollution formation seismology [8,9]. Zeolites, metal MXenes, metal oxides, conducting polymers, and other materials are used in dye treatments. Due to their remarkably high surface area and superior semiconducting properties, many transition metals and their oxide nanoparticles have been synthesized and tested for photocatalytic performance. Metal oxides such as ZnO, CuO, TiO_2, AgO, and Co_3O_4 are commonly used in photocatalytic dye degradation [8–12].

Among these, Co_3O_4 in particular demonstrated an impressively extensive application for catalysts, sensors, magnetic materials, and energy storage electrode materials [12]. The methods used to prepare these metal oxides, such as sol-gel, hydrothermal, electrochemical, solvent evaporation, co-precipitation, and green synthesis, are extensively used. Among them, green synthesis is a low-cost, environmentally friendly, and simple method for producing metal oxide nanoparticles [13]. Many green-mediated metal oxide syntheses are ZnO, Fe_2O_3, AgO, CuO, and Al_2O_3 using plant sources such as Agathosma betulina, Sida cordifolia, Pedalium murex, Gloriosa superba, and Prunus yedoensis [14]. *Curcuma longa* is a tropical rhizomatous mostly extensively cultivated in India. The medicinal benefits of *Curcuma longa* include anti-inflammatory, antimicrobial, antiseptic, anti-fungal, antiallergenic, antioxidant, anthelmintic, antimalarial, antiallergic activity, antiarthritic, antiulcer, antidiabetic, antiaging, anti-mutagenic and anti-cancer activity [15–19]. For the green synthesis of metal oxide using curcumin as a reducing agent for different nanoparticle preparations by assembling the work presented in many works of literature. In general, green synthesis involves two vital steps in the synthesis of nanoparticles. Curcumin, as a reducing agent, provides metal reduction from M^{x+} to M^0 while also stabilizing the formation of arbitrary aggregation and controlling the size and shape of the nanoparticles [20–22].

The present work focuses on three major points, which are: (i) The metal oxide Co_3O_4 nanoparticles are constructed using green synthesis curcumin extract. The plant extract helps to attain the nanostructure formation, reduced the light recombined activity and increased the ROS activities. (ii) Organic contaminants of MB dye were removed from aquatic surfaces through the photocatalysis method under visible light irradiation. Bacterial strains of *E. coli* and *S. aurues* are eradicated by using Co_3O_4 nanoparticles.

2. Materials and Methods

2.1. Materials

Cobalt nitrate hexahydrate ($Co(NO_3)_2$. $6H_2O$) and Methylene Blue ($C_{16}H_{18}ClN_3S$) was acquired from HiMedia, Mumbai, India. The purchased chemicals were obtained at 99.9% purity in analytical reagent (AR) grade, and no extra refinement occurred in the synthesis time. The fresh leaf of the *Curcuma longa* plant was collected from Kerala, India.

2.2. Plant Extract Preparation

The *Curcuma longa* plant leaves (5 g of fresh leaves) were washed with running tap water. The round bottom flask was used to combine the cleaned green leaf and 100 mL double distilled water. The combinations of leaf and distilled water were heated for 30 min at 60 °C, and Whatman No. 1 filter paper was used to filter the sediment. The obtained pure leaf extract solution was kept at 4 °C conditions for further evolutions.

2.3. Biosynthesis of Co_3O_4 Nanoparticles

0.1 M Cobalt nitrate hexahydrate ($Co(NO_3)_2$. $6H_2O$) and 10 mL plant extract of *Curcuma longa* were used in the nanoparticle synthesis process. Both sources were mixed by using a magnetic stirrer at constant rpm (750 rpm) for 30 min. The color deviations from light brown to dark brown specify the nucleation and growth of Co_3O_4 nanoparticles. The obtained color-modified nanoparticle solutions were centrifuged at 10,000 rpm for 10 min (repeated three times), and their obtained pellet was washed with double distilled water. Finally, the collected nanoparticle precipitate was filtered (with Whatman No. 1 filter paper) and dried in the oven at 100 °C for 60 min. The dried nanoparticle samples were processed for further measurements [23,24].

2.4. Characterization of Nanoparticles

Structural phase and material crystallinity are evaluated from XRD (PANalytical X'Pert Pro Diffractometer; radiation = Cu Kα (1.5405 Å); working condition = 30 kV and 40 mA) analysis. The nanoparticle formation, reaction, and functional group involvement were captured by Perkin Elmer FT-IR spectroscopy, and their wavelength limit is 4000 cm^{-1} to 400 cm^{-1}. The optical imperfections and their transition properties were observed from UV-visible DRS (UV-2600 Shimadzu) analysis. The nano-sized surface structural modification and their elemental compositions were analyzed from FESEM (Carl Zeiss) and TEM (Titan) with EDX spectroscopy. The valency, bonding, and binding energies of the synthesized nanoparticles were characterized by using x-ray photoelectron spectroscopy (XPS; PHI 5000 Versa Probe III, Physical Electronics, Chanhassen, USA) [23,24].

2.5. Photocatalytic Activity

The photocatalytic activity of biosynthesized Co_3O_4 nanoparticles was examined using the organic effluent of MB dye. The visible light source (Xenon lamp wavelength = 400 nm) irradiated the Co_3O_4 nanoparticles. The 10 mg of Co_3O_4 nanoparticles were mixed with 100 mL (10-ppm) of MB dye solution by using a magnetic stirrer and kept in a dark environment for 40 min. The dark condition stirring process helps to attain the adsorption-desorption equilibrium positions. Visible light photocatalytic activity of Co_3O_4 nanoparticles and dye solution were processed by closed chamber xenon lamp irradiation. The light irradiation dissociated the dye bonding and decreased the absorbance strength over the catalyst; it was measured at 10 min intervals. 10 min time gap, the dye solution was taken out and centrifuged for 1000 rpm to remove the catalyst from the dye solution and measured in UV-Visible spectroscopy. The dissociated dye absorbance was calculated [25–27].

2.6. Antibacterial Activity

The microbial resistance of Co_3O_4 nanoparticles was measured in gram-positive *Staphylococcus aureus* (ATCC 6538) and gram-negative *Escherichia coli* (ATCC 8739) through

the well diffusion method. The 10^6 CFU/mL concentrated bacterial culture was inoculated into the nutrient broth and placed in the incubator for overnight incubation. The Muller-Hinton agar medium was poured into sterilized Petri plates and incubated overnight, and the growing culture was swabbed on the sterilized Petri plates. The 5 mm holes were made by the gel puncture method in the Muller-Hinton agar plates, and the holes were filled with different concentrations of Co_3O_4 nanoparticles (10, 20, 50, and 100 µg/mL) nanoparticles. Then, the plates were incubated at 37 °C for 24 h. The cell death and deactivation were assessed by the development of a clear zone around the holes, which was measured on a millimeter (mm) scale [27].

3. Result and Discussions

3.1. XRD Analysis

The biosynthesized Co_3O_4 nanoparticles' x-ray diffractive pattern is presented in Figure 1. The diffraction peaks of Co_3O_4 nanoparticles appearing at 2θ = 19.00°, 31.008°, 36.88°, 44.72°, 59.18°, and 65.19° can be assigned to the (111), (220), (311), (222), (400), and (511) planes. The obtained Co_3O_4 nanoparticles peaks are well-coincided with the cubic structure of standard JCPDS card number 042-1467 [28]. The bio-molecule interaction on the cobalt sources exhibited the cobalt and oxygen nucleation sites and attracted each other by electron donor of plant molecules, which derived the Co_3O_4 nanoparticles. The high-intensity peak of 36.88° represents the high crystallinity and lattice strain of Co_3O_4 nanoparticles. The crystallite size of Co_3O_4 nanoparticles was determined by using the Debye-Scherrer formula [29]. The obtained 26 nm, the crystallite size of cubic Co_3O_4 nanoparticles, derived the narrow crystallite size, and it emanated the high electron accumulation of the surfaces. The smallest crystallite size increased the surface area, which enhanced the degradation capability of the hazardous dyes and organic substances.

3.2. FTIR Analysis

The Co_3O_4 nanoparticle purity, plant extract bio-molecule qualitative measurement, and surface modifications were determined by FTIR spectroscopy and displayed in Figure 2. The cobalt oxide nanoparticles FTIR spectrum derived the cobalt, oxygen and reaction involved plant nutrients. FT-IR results for plant extract revealed absorption bands at 3261 cm^{-1} and 1636 cm^{-1}. The broad peak at 3261 cm^{-1} indicates O-H stretching vibrations and absorbed water molecules in the plant extract. The sharp peak at 1636 cm^{-1} indicates the presence of amides. The phytochemicals, such as terpenoids, alkaloids, phenols, steroids, and flavonoids, are mostly found in the *C. longa* extract. After the addition of *C. longa* leaf extract to the cobalt nitrate solution, the color change indicates the formation of Co_3O_4 nanoparticles. Curcumin, one of the major polyphenolic compounds found in the *C. longa* plant, might be involved in the synthesis of copper oxide and nickel oxide nanoparticles. Herein, the Co^{2+} ions were reduced to form Co_3O_4 nanoparticles by donating the electrons from curcumin. The broad two prominent peaks are indicating the formation of Co_3O_4 nanoparticles at 555 cm^{-1} and 659 cm^{-1} [30,31]. Co(III)-O bonds were obtained from 659 cm^{-1} Co-O stretching vibrations associated with 555 cm^{-1}. The plant extract produced amide and carboxylic acid on the cobalt materials, which can be used for the reduction, capping, and stabilization of Co_3O_4 nanoparticles [32,33]. The minor peaks of 1382 cm^{-1} and 1639 cm^{-1} denote the amide and carboxylic acid from plant biomolecules. The water molecule and carbon attachment on the surfaces were observed from the peaks of 2331 cm^{-1} and 3415 cm^{-1} it representing the -OH stretching and C=O asymmetric vibration of the CO_2 molecule [34–36]. The existing carbon and OH molecules are responsible for the reduction and enhanced activity of Co_3O_4 nanoparticles.

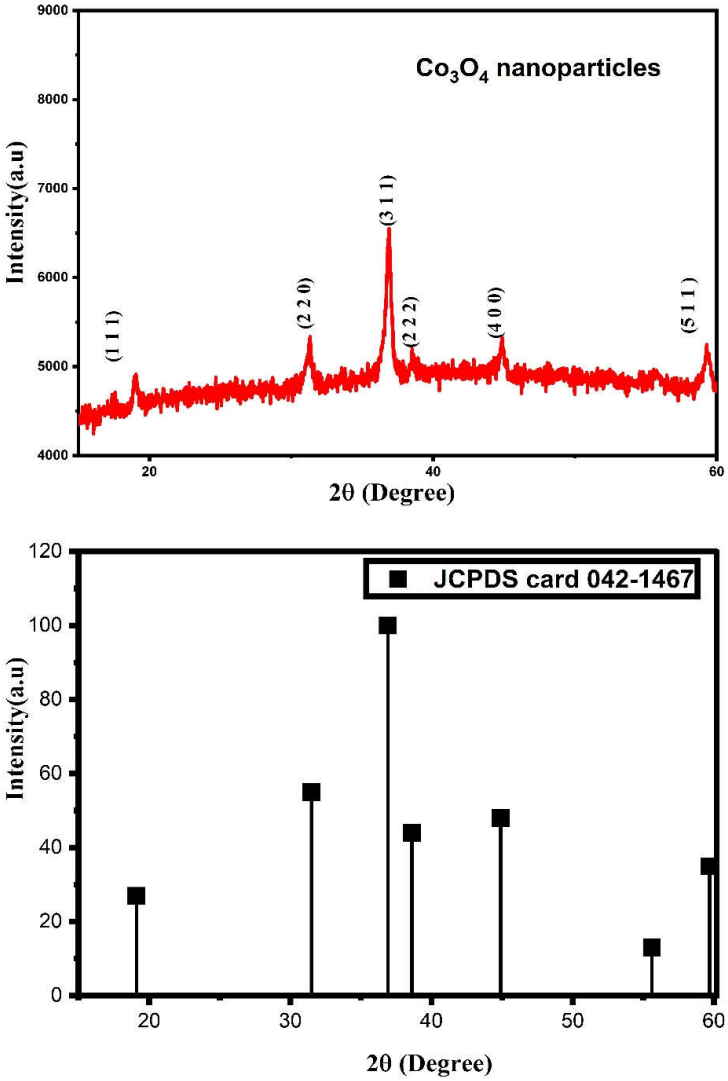

Figure 1. X-ray diffraction pattern of Co_3O_4 nanoparticles.

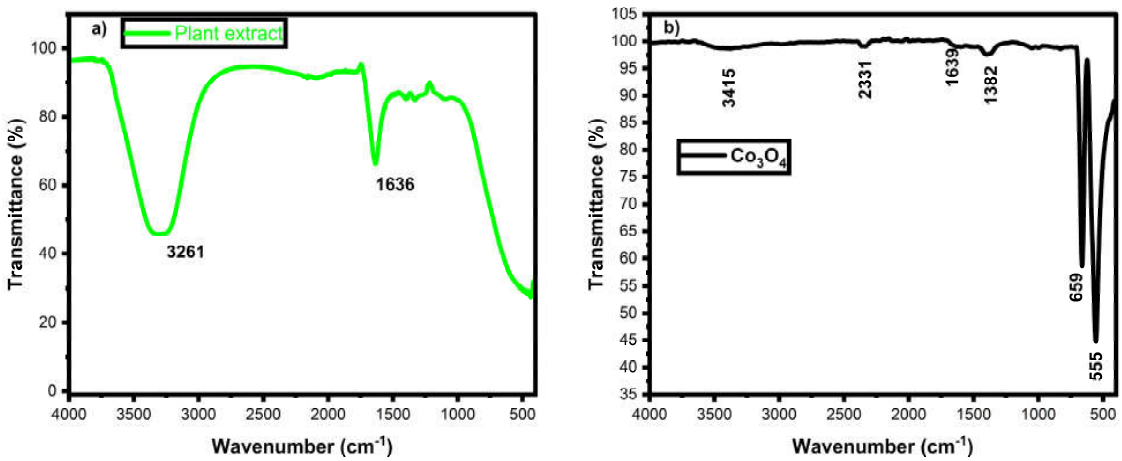

Figure 2. FTIR spectrum of *C. longa* (**a**) and Co_3O_4 nanoparticles (**b**).

3.3. UV-DRS Analysis

The absorbance and bandgap spectra of green-mediated Co_3O_4 nanoparticles are displayed in Figure 3. The green-mediated Co_3O_4 nanoparticles establishment was identified from the absorbance peaks at 380 and 690 nm [37,38]. Broad two-peaks from green-

mediated Co_3O_4 nanoparticles elucidated the transition of charges from O to Co orbitals. Co^{2+} and Co^{3+} orbital electrons move towards the O^{2-}, which indicates the double oxidation state of cobalt elements [37,38]. P-type green-mediated Co_3O_4 nanoparticles optical imperfections were derived from Kubelka-Munk relations. Green-mediated Co_3O_4 nanoparticles calculated bandgap is 3.4 eV, which was well matched with previously reported Co_3O_4 nanoparticles [39]. The wide bandgap of Co_3O_4 nanoparticles explained the gap between the holes and electrons, which suppressed the recombined activity. The obtained photo exciton charge carriers provoke the oxygen vacancy on the Co_3O_4 nanoparticles [39]. The charge carrier mitigations and partings may deduce the organic pollutants and deactivate the bacterial system in wastewater and biomedical applications.

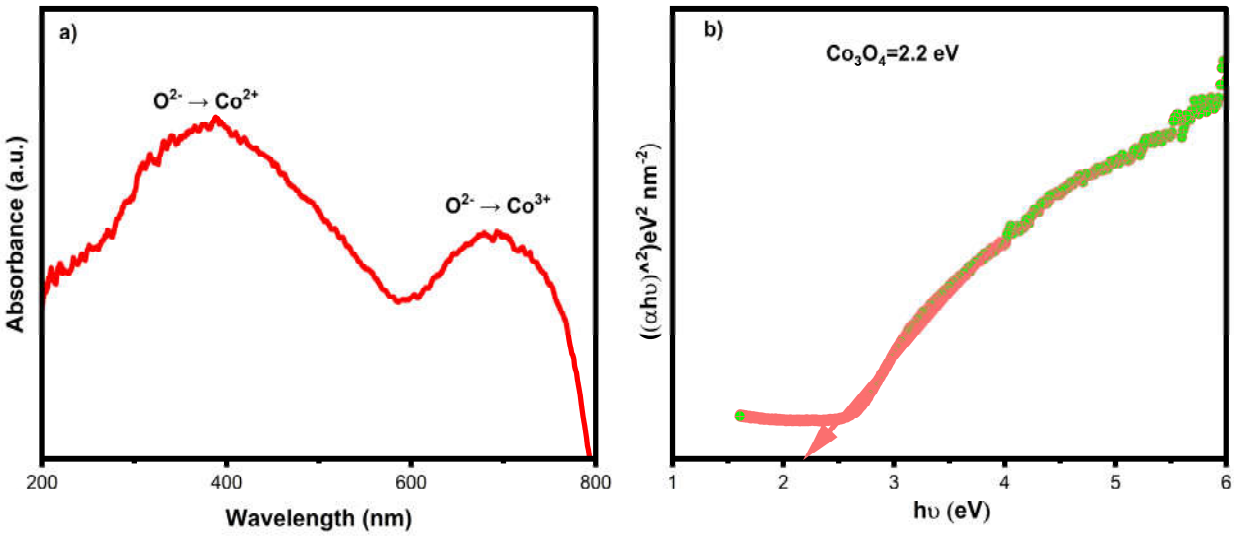

Figure 3. UV-DRS absorbance (**a**) and bandgap energy (**b**) spectrum of Co_3O_4 nanoparticles.

3.4. FESEM with EDX Analysis

Surface morphological and elemental analysis of biogenic synthesized Co_3O_4 nanoparticles studied by FESEM with EDX and their belongings are displayed in Figure 4a–d. Spherical-shaped and mixed spherical nanoparticle morphologies were observed in biogenically synthesized Co_3O_4 nanoparticles. The spherical shape of Co_3O_4 nanoparticles was achieved through the nucleation, growth, and aggragation of the synthesized materials. Mixed shaped Co_3O_4 nanoparticles were obtained from the aggomeleration of synthesized Co_3O_4 nanoparticles due to the capped plant molecules. Plant derivatives controlled the nucleation, growth, and structuring of nanoparticles, and their enriched quantities of phytonutrients agglomerated the biogenically synthesized Co_3O_4 nanoparticles [40,41]. Metal and oxygen stabilization/interface formed the nanostructure of biogenically synthesized Co_3O_4 nanoparticles. EDX spectroscopy of biogenically synthesized Co_3O_4 nanoparticles confirmed the existing elements of Co and O (Figure 4c,d). Their Co and O presence elucidates the phase of pure biogenically synthesized Co_3O_4 nanoparticles, and no other element is evolved in the reactions. Metal compound occurrence is high in the biogenically synthesized Co_3O_4 nanoparticles because of their lattice oxygen stabilization [41–43]. Further, the oxygen vacancy was stabilized and filled by cobalt cations, and their values are presented in Figure 4d.

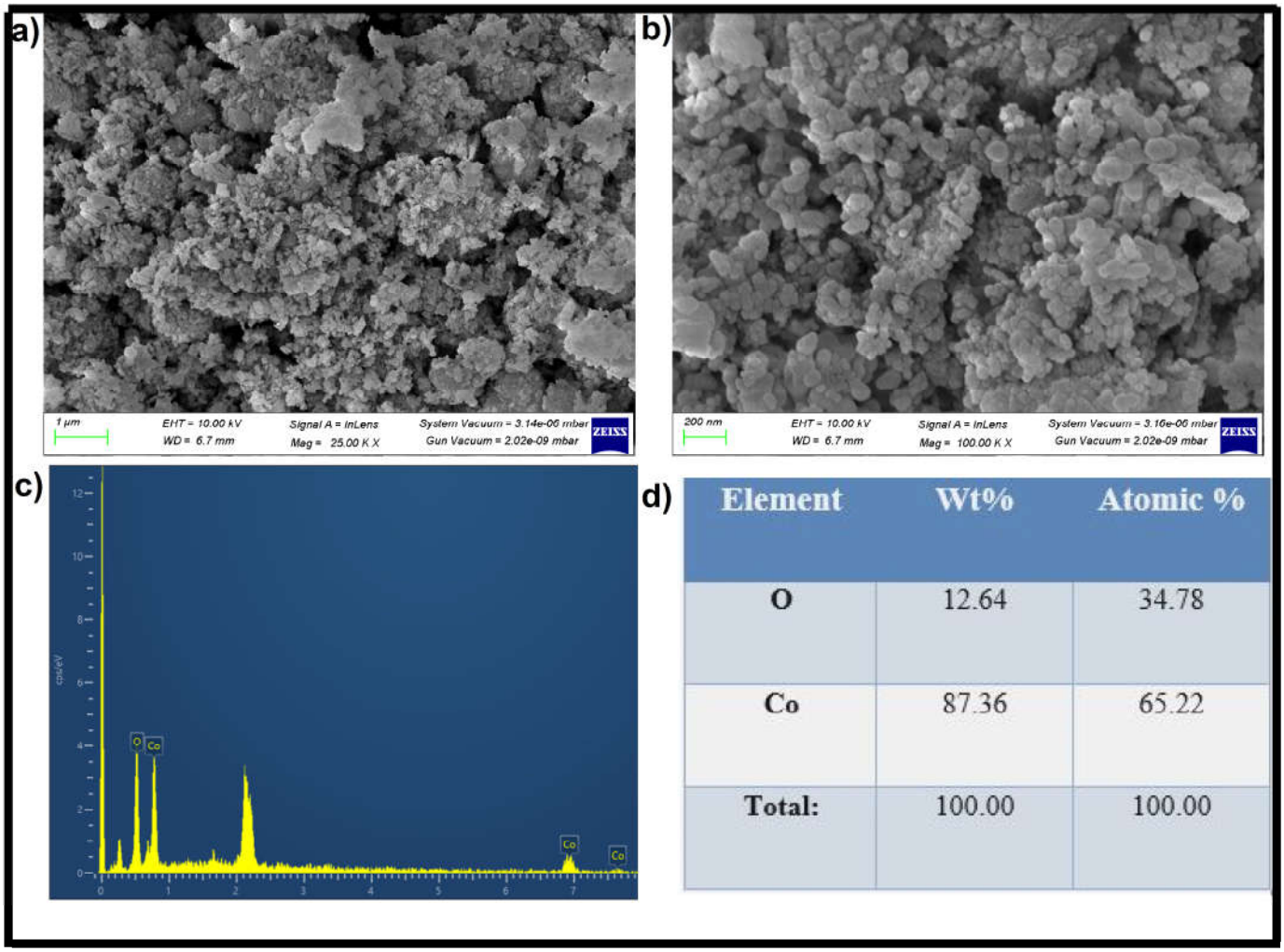

Element	Wt%	Atomic %
O	12.64	34.78
Co	87.36	65.22
Total:	100.00	100.00

Figure 4. FESEM images (**a**,**b**), EDX peak spectrum (**c**) and EDX table (**d**) of Co_3O_4 nanoparticles.

3.5. TEM Analysis

The TEM analysis examined the surface morphology and particle size of the biogenically synthesized Co_3O_4 nanoparticles. The two different magnifications with two different parts of biogenically synthesized Co_3O_4 nanoparticles are exhibited in Figure 5a,b. The biogenically synthesized Co_3O_4 nanoparticles revealed the spherical shape and lite black surroundings over spherical and conjoint spherical shapes representing the plant molecules encapsulations [44,45]. The plant molecule encapsulations over the biogenically synthesized Co_3O_4 nanoparticles are relieved from FTIR and XPS analysis. The particle size of biogenically synthesized Co_3O_4 nanoparticles is 22 nm. The obtained particle size values denoted the lattice constraint between the cobalt and oxygen, and their electron mobilization was evident from XRD and UV-DRS analysis.

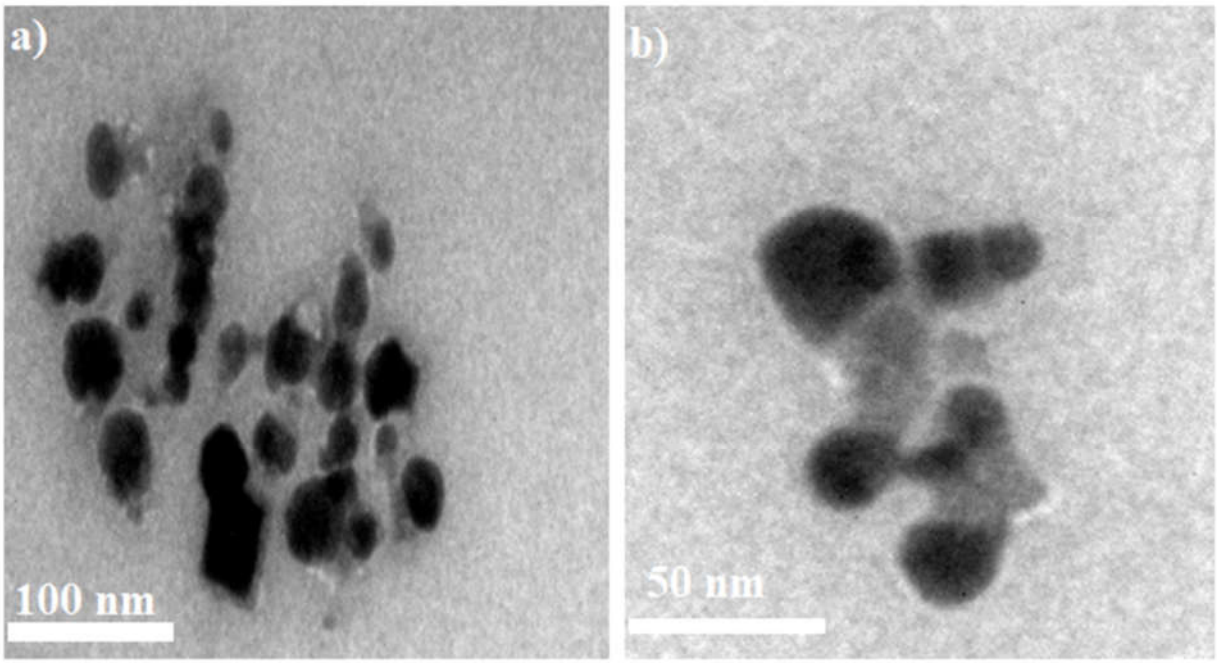

Figure 5. Different magnified TEM images of ((**a**)-100 nm and (**b**)-50 nm) Co_3O_4 nanoparticles.

3.6. XPS Analysis

The XPS analysis examined the chemical valency and binding energy of the biogenically synthesized Co_3O_4 nanoparticles. The valency of the material is determined by the catalytic efficiency of the synthesized compounds. The XPS spectrum displays the wide, Co, O, and C elements from biogenically synthesized Co_3O_4 nanoparticles, as displayed in Figure 6a–d. A wide spectrum of biogenically synthesized Co_3O_4 nanoparticles presented Co, O, and C elements (Figure 6a). The Co and O elements confirmed the formation of Co_3O_4 nanoparticles, and the C elements come from plant extract. The Co elements are represented by two major peaks and their Co-2p state existence in 796 eV = Co-$2p_{1/2}$ and 780.2 eV = Co-$2p_{3/2}$ respectively (Figure 6b). The Co double splitting is well documented with the previously reported work and standard Co element [46,47]. The O spectrum is located at 529–531 eV, and its valency is O-1s (Figure 6c). The lattice oxygen peaks complete the reaction of the biogenically synthesized Co_3O_4 nanoparticles, and their interface was led by the plant nutrients [46]. The cationic metals interacted with the organic plant molecules, and they could create oxygen vacancies on the surfaces. Three peaks were obtained in the O-1s XPS spectrum, including lattice oxygen, surface oxygen, and oxygen defect. The oxygen spectra determined the robust interface between metal and plant organic molecules. The absorbed oxygen on cationic metal is established the metal oxide nanostructure [47]. The plant extract reduced the zero valent cobalt and re-oriented it with lattice oxygen, which formed the biogenically synthesized Co_3O_4 nanoparticles. The bio-reduction of the biogenically synthesized Co_3O_4 nanoparticles was assured by the C-1s peak (Figure 6d). The three different small peaks are depicted in the C-O, C-C, and C=O bonds, which provoke the reduction and stabilization of Co and O elements to produce the biogenically synthesized Co_3O_4 nanoparticles [47,48]. Further, the attained findings confirmed the high-purity biogenic synthesized Co_3O_4 nanoparticles.

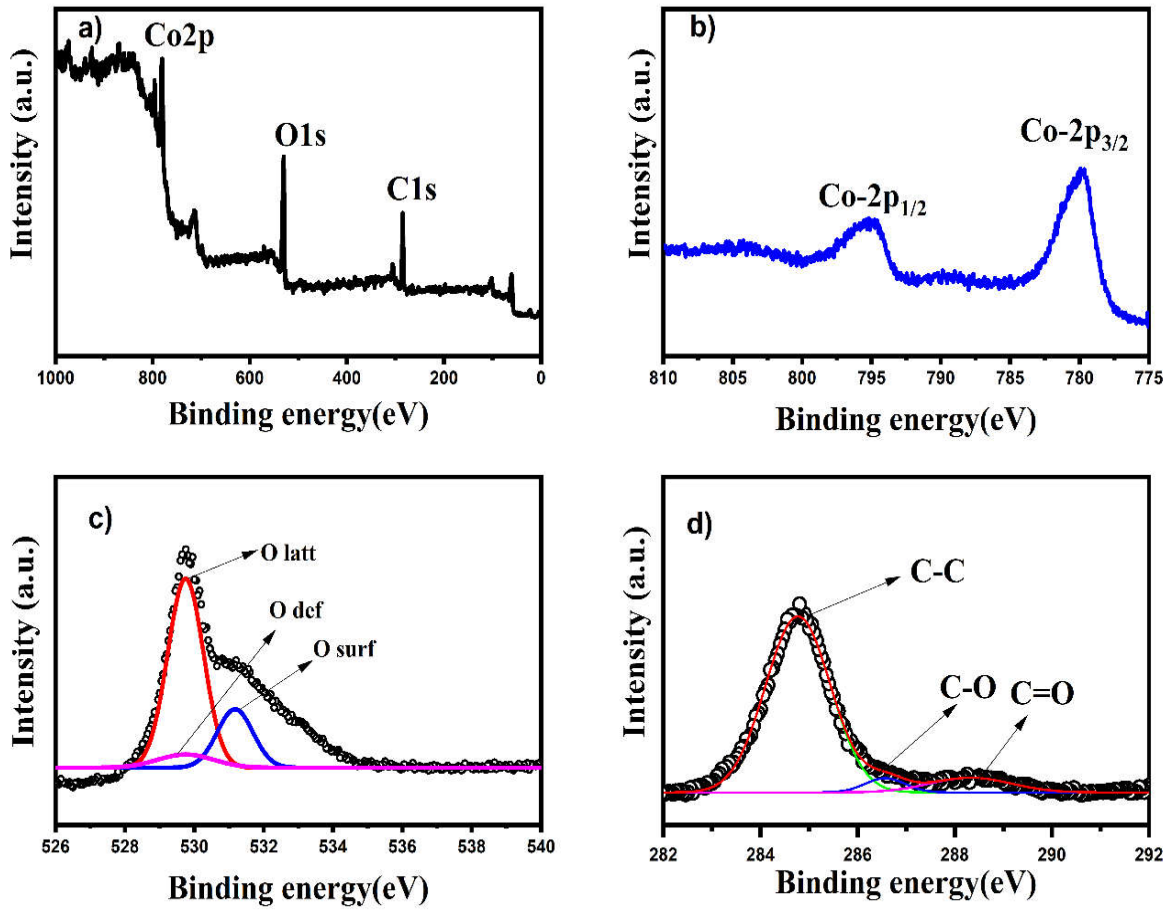

Figure 6. XPS of Co_3O_4 nanoparticles wide (**a**), cobalt (**b**), oxygen (**c**) and carbon (d) spectrum.

3.7. Photocatalytic Dye Degradation

Photocatalytic degradation of MB was studied using as-synthesized Co_3O_4 nanoparticles under visible light irradiation. The visual color of the treated dye and UV-vis spectrum are shown in Figure 7a. In this present case, the photocatalyst, Co_3O_4 nanoparticles, has a complex spinel structure in which Co^{2+} ions occupy tetrahedral sites and Co^{3+} ions occupy octahedral sites of the cubic close-packed lattice of oxide anions [49]. The valance band is characterized by the (2p) orbital having O_2^- carriers, whereas the 3d orbital contributes Co^{2+} carriers in the conduction band. As a result, the charge transfer band (O_2^- to Co^{2+}) that appears in the wavelength range 400–800 nm is the primary governing factor for Co_3O_4 nanoparticle-based photocatalytic processes. When photons were illuminated, the methylene blue dye produced reactive species that inserted electrons back into the lattice plane of Co_3O_4 nanoparticles, assisting in the creation of superoxide radicals in the presence of accessible oxygen in the solution, further enhancing the photodegradation process. The breakdown of the chromophoric group and the transformation of dye into low molecular weight by-products are connected with the photocatalytic degradation of the target dye [50]. Under visible light irradiation, dye degradation is primarily caused by the creation of electrons (e^-) and holes (h^+) on the catalyst surface. Water molecules mix with holes h^+ to form the OH radical. The O_2 molecule scavenges the electrons e^- and converts them to OH through HOO and H_2O_2 intermediates. The OH is a powerful oxidizing species that non-selectively degrades the organic molecule dye into H_2O, CO_2, and inorganic ions [51]. The same work was repeated three times with the same experimental conditions, and their standard deviation values were calculated. The MB dye degradation (90%) during the 40-min radiation exposure is depicted in figure (b). The rates of methylene blue degradation using Co_3O_4 photocatalyst were determined from the graph of ln(Co/Ct) vs time (min). The kinetic study infers the pace of the order of the reaction. The graph depicts a straight

line with a positive slope and a rate constant of 0.05468 min^{-1} for Co_3O_4 nanoparticles. The mechanism of photodegradation is shown in Equations (1)–(7).

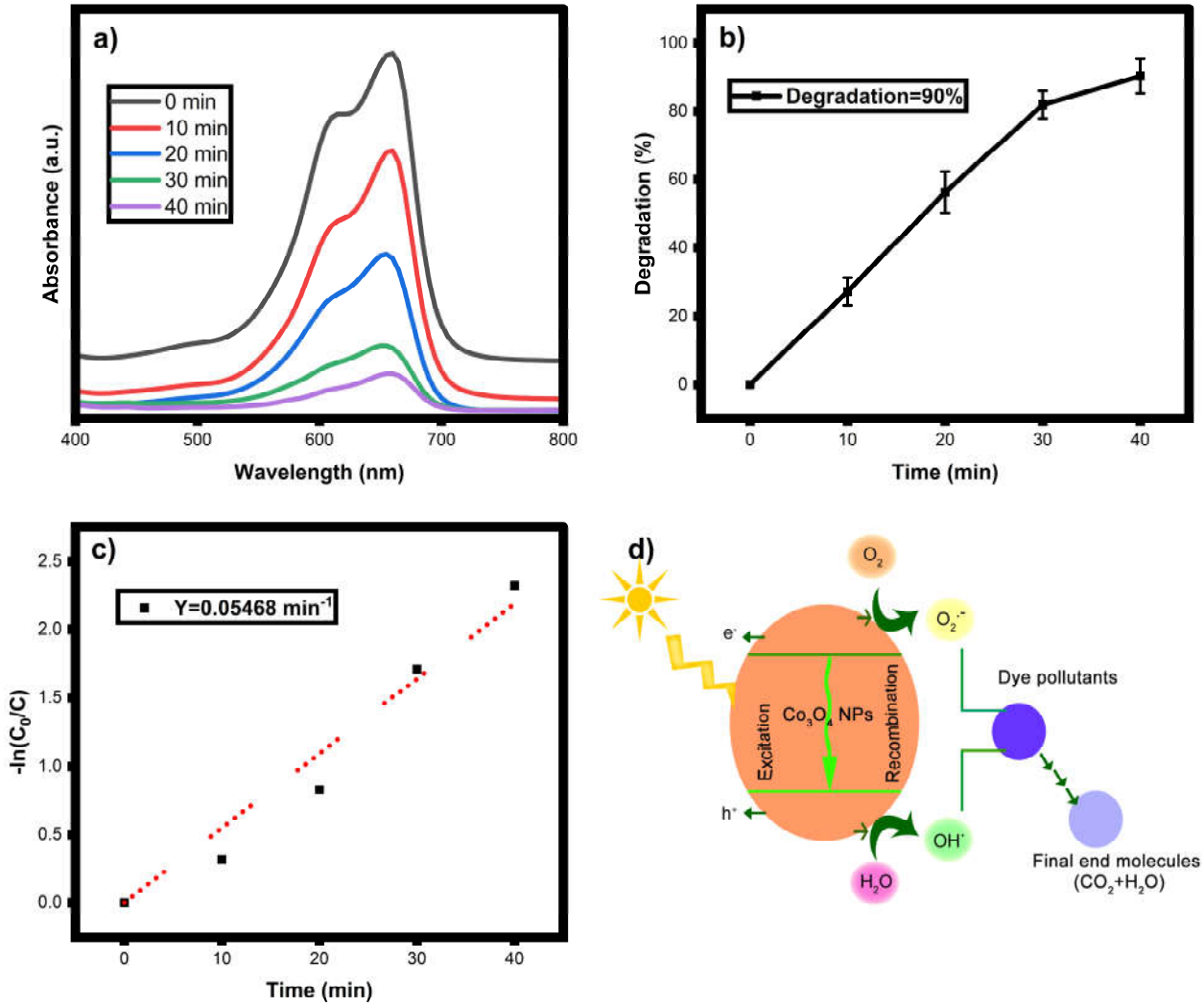

Figure 7. (**a**) Visible light MB dye degradation spectrum, (**b**) Degradation efficiency, (**c**) kinetic rate and (**d**) Photocatalytic dye degradation mechanism of Co_3O_4 nanoparticles.

3.8. Photodegradation Mechanism

The degradation of organic pollutants is influenced by various parameters such as light source, surface area, bandgap, sizes, ion releasing capacity, dye concentration and catalyst dosage etc. The cobalt oxide nanoparticle degradation of various dye solutions is listed in Table 1. The present work degradation efficiency is compared with previous reported work, and the obtained degradation is expressed as the enhanced degradation potential of published work [52–61].

$$\mathbf{Co_3O_4 + light\ energy \rightarrow h^+ + e-} \quad (1)$$

$$\mathbf{H_2O + h^+ \rightarrow H^+ + OH} \quad (2)$$

$$\mathbf{e^- + O_2 \rightarrow O_2{}^-} \quad (3)$$

$$\mathbf{H^+ + O_2{}^- \rightarrow HOO} \quad (4)$$

$$\mathbf{HOO \rightarrow O_2 + H_2O_2} \quad (5)$$

$$\mathbf{H_2O_2 \rightarrow OH} \quad (6)$$

$$\textbf{OH + Dye} \rightarrow \textbf{Dissociated dye products} \quad (7)$$

Table 1. Comparison table of Co_3O_4 nanoparticles degradation against different conditions.

S.No	Sample	Dye	Dye volume	Dosage	Degradation (%)	References
1.	Co_3O_4	MB	50 mL	0.1 mg	93.8	[52]
2.	Co_3O_4	TY	100 mL	0.0020 g	51.4	[53]
3.	Co_3O_4	BO	100 mL	0.5 g	78.45	[54]
4.	Co_3O_4	MV, CV	50 mL	1.0 g	92 and 64	[55]
5.	Co_3O_4	MG	100 mL	50 mg	91.2	[56]
6.	Co/Co_3O_4	AR and AB	50 mL	0.04 g	93 and 69.5	[57]
7.	Co and Co_3O_4	murexide dye and EBT	100 mL	0.1 gL^{-1}	43 and 39	[58]
8.	Co_3O_4	CR	100 mL	0.50 g	98	[59]
9.	Co_3O_4	MB	20 mL	5 mg	86	[60]
10.	Co_3O_4	MO	100 mL	6 mg	95	[61]
11.	**Co_3O_4**	**MB**	**100 mL**	**10 mg**	**90**	**Present work**

Effect of Catalyst Dosage

The various catalyst dosages were scrutinized against the MB dye solution. The photocatalytic dye degradation of various catalyst concentrations was demonstrated in Figure 8. A low catalyst dosage of 1 mg causes 58% degradation and 5 mg causes 69% degradation against MB dye. The excitation of electrons and light absorption is based on the catalyst surface area, and it can be motivated by radical genericity. 10 mg catalyst dosage is optimized concentrations of Co_3O_4 nanoparticles than 1 mg, 5 mg and 15 mg (71%) Co_3O_4 nanoparticles. The high surface area and OH radical productivities destroyed the dye bonding and increased the active sites of the nanomaterial surfaces. The 15 mg of Co_3O_4 nanoparticles restricted the electron mitigations from different bands due to their high occupations, which do not allow light movements that can suppress the charge carrier multiplicity. Therefore, 10 mg of Co_3O_4 nanoparticles are produced for improved photocatalytic dye degradation.

3.9. Antibacterial Activity

Bacterial contamination leads to a variety of issues for all, such as infection, mortality, and organ defects, which are controlled by antibiotics. The high usage of antibiotics is expressed by the many irregularities and the complete suppression of the bacterial domains. Good bacteria are also degraded by antibiotics, and their long-term use inhibits the nerve action system. Hence, researchers are focusing to raise innovative techniques to reduce the hazardous evolution and dispersion. Nanophase materials are always a new and effective antibacterial output for the scientific community. Biogenic nanoparticles give a superior bacterial resistive property in various bacterial strains [62]. The present study of biogenic Co_3O_4 nanoparticles showed significant bacterial output against *E. coli* and *S. aureus* bacterial strains. The results of using Co_3O_4 nanoparticles showed an increased zone of inhibition with increasing nanoparticle concentrations [63–65]. The inhibited bacterial plate was shown in Figure 9. The statistical analysis of the Co_3O_4 nanoparticles antibacterial activity was calculated. The zone of inhibitions tells the sensitivity and resistivity of Co_3O_4 nanoparticles. Gram-positive bacteria of *S. aureus* have a higher effective sensitivity than gram-negative bacteria of *E. coli*. The lipopolysaccharide protected cell wall could not be easily destructed by the metal ions due to its thickness. Peptidoglycan-covered cell wall bacterial strains are easily penetrated by nanoparticles due to their 80 nm layered thickness of the cell wall [62–66]. This is the main reason for the metal ions entry into the interactions of the bacterial structure. The disrupted cell wall permits the Co_3O_4 nanoparticles, and it provokes ROS production. Increased toxic levels in the cell system suppressed the nucleus

and DNA production. Without nutrients, a cell body lost its energy, which stopped the cell active signaling and induced the cell demise.

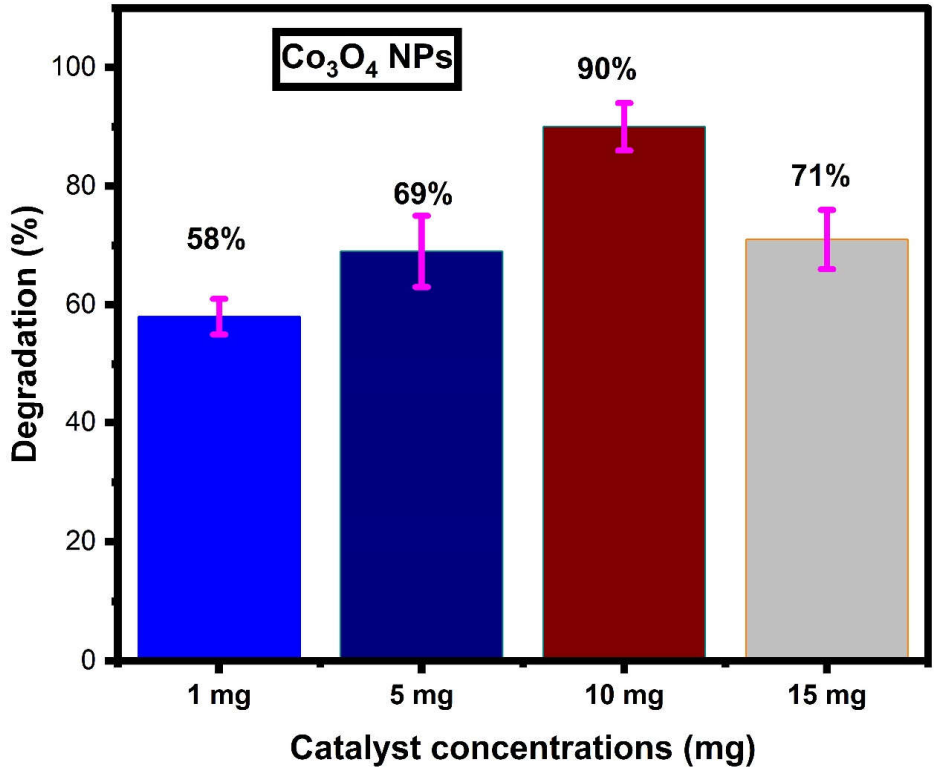

Figure 8. Effect of catalyst dosage on Co_3O_4 nanoparticles.

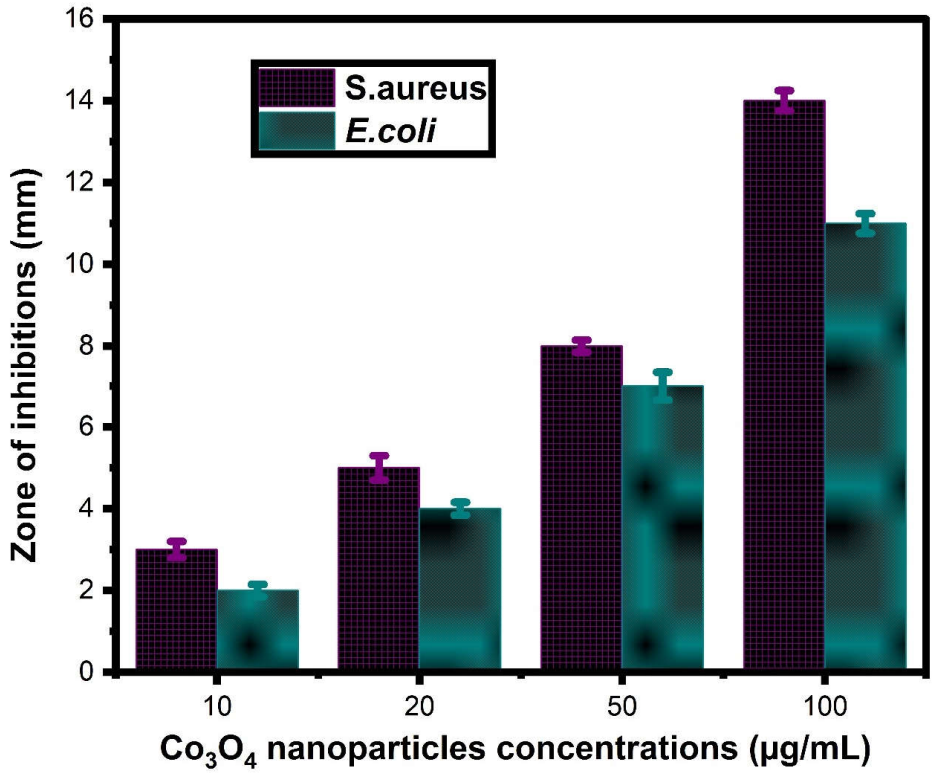

Figure 9. Antibacterial activity of Co_3O_4 nanoparticles against *S. aureus* and *E. coli* with different concentrations.

4. Conclusions

Bio-mediated nanophase material constructions are gaining extra attention in all research sectors due to their noxious, cost-effective, and pollution-free method of synthesis. *Curcuma longa* plant extract achieved the in-situ reduction of valence-free cobalt atoms and encouraged lattice oxygen stabilizations. The crystallite size and spherical morphologies of the *Curcuma longa*-derived Co_3O_4 nanoparticles designate their 26 nm size and a large area on the surfaces of the Co_3O_4 nanoparticles. The optical and chemical valency of the Co_3O_4 nanoparticles projected the Co^{2+} and Co^{3+} valency over the oxygen vacancies. Electronic transitions of Co_3O_4 nanoparticles specify the formation of Co and O stabilization and improved the material interface by plant extract of *Curcuma longa.* Biogenic Co_3O_4 nanoparticles exhibited enhanced antibacterial efficiency in gram-positive bacterial strains. Visible light photocatalytic dye degradation activity of Co_3O_4 nanoparticles was investigated against MB dye under and obtained the degradation is 90%. The double valency of Co_3O_4 nanoparticles increases the lifetime of electron-hole pair recombination and intensifies the oxidation and reduction properties against the MB dye. Therefore, oxidation of Co_3O_4 nanoparticles enhanced the parting of charge particles, enlarged the radical speciation, and produced noxious-free end products. Consequently, obtained results advocate the Co_3O_4 nanoparticles can be used for further growth and applications in the water-treatment process and biomedical-related areas.

Author Contributions: Conceptualization, P.C. and S.M.W.; methodology, P.C.; software, H.P.S. and H.S.M.; validation, P.C, A.I. and S.M.W.; formal analysis, P.C.; investigation, P.C.; re-sources, M.M.R.A.K., H.S.M., M.J.J., A.I., S.M.W. and W.-C.L.; data curation, A.I.; writing—original draft preparation, P.C.; writing—review and editing, P.C., S.M.W., A.I., W.-C.L. and M.J.J.; visualization, P.C.; supervision, P.C.; project administration, P.C.; funding acquisition, S.M.W. and W.-C.L. All authors have read and agreed to the published version of the manuscript.

Funding: The authors are grateful to the Researchers Supporting Project No. (RSP2023R448), King Saud University, Riyadh, Saudi Arabia.

Institutional Review Board Statement: Not applicable.

Informed Consent Statement: Not applicable.

Data Availability Statement: All research data are associated with the manuscript.

Acknowledgments: The authors are grateful to the Researchers Supporting Project No. (RSP2023R448), King Saud University, Riyadh, Saudi Arabia. Parvathiraja Chelliah is thankful to the V.O.Chidambaram College, Thoothukudi, Tamilnadu, and Sadakathullah Appa College, Tirunelveli, Tamilnadu, India.

Conflicts of Interest: The authors declare no conflict of interest.

References

1. Ismail, M.; Akhtar, K.; Khan, M.I.; Kamal, T.; Khan, M.A.; Asiri, A.M.; Seo, J.; Khan, S.B. Pollution, Toxicity and Carcinogenicity of Organic Dyes and their Catalytic Bio-Remediation. *Curr. Pharm. Des.* **2019**, *25*, 3645–3663. [CrossRef] [PubMed]
2. Burkinshaw, S.M. Application of dyes. In *The Chemistry and Application of Dyes*; Springer: Boston, MA, USA, 1990; pp. 237–379.
3. Gregory, P. Classification of Dyes by Chemical Structure. In *The Chemistry and Application of Dyes*; Springer: Boston, MA, USA, 1990; pp. 17–47. [CrossRef]
4. Mondal, P.; Baksi, S.; Bose, D. Study of environmental issues in textile industries and recent wastewater treatment technology. *World Sci. News* **2017**, *61*, 94–105.
5. Moradi, O.; Pudineh, A.; Sedaghat, S. Synthesis and characterization Agar/GO/ZnO NPs nanocomposite for removal of methylene blue and methyl orange as azo dyes from food industrial effluents. *Food Chem. Toxicol.* **2022**, *169*, 113412. [CrossRef]
6. Harvey, J.W.; Keitt, A.S. Studies of the efficacy and potential hazards of methylene blue therapy in aniline-induced methaemoglobinaemia. *Br. J. Haematol.* **1983**, *54*, 29–41. [CrossRef] [PubMed]
7. Mohammed, M.; Shitu, A.; Ibrahim, A. Removal of methylene blue using low cost adsorbent: A review. *Res. J. Chem. Sci. ISSN* **2014**, *2231*, 606X.
8. El-Sharkawy, E.; Soliman, A.Y.; Al-Amer, K.M. Comparative study for the removal of methylene blue via adsorption and photocatalytic degradation. *J. Colloid Interface Sci.* **2007**, *310*, 498–508. [CrossRef]
9. Entezari, M.; Sharifalhoseini, Z. Sono-sorption as a new method for the removal of methylene blue from aqueous solution. *Ultrason. Sonochem.* **2007**, *14*, 599–604. [CrossRef]

10. Sarioglu, M.; Atay, U.A. Removal of methylene blue by using biosolid. *Glob. Nest J.* **2006**, *8*, 113–120.
11. Julkapli, N.M.; Bagheri, S.; Hamid, S.B.A. Recent Advances in Heterogeneous Photocatalytic Decolorization of Synthetic Dyes. *Sci. World J.* **2014**, *2014*, 692307. [CrossRef]
12. Ahuja, P.; Ujjain, S.; Kanojia, R.; Attri, P. Transition Metal Oxides and Their Composites for Photocatalytic Dye Degradation. *J. Compos. Sci.* **2021**, *5*, 82. [CrossRef]
13. Suresh, S.; Vennila, S.; Anita Lett, J.; Fatimah, I.; Mohammad, F.; Al-Lohedan, H.A.; Alshahateet, S.F.; Motalib Hossain, M.A.; Rafie Johan, M. Star fruit extract-mediated green synthesis of metal oxide nanoparticles. *Inorg. Nano-Met. Chem.* **2022**, *52*, 173–180. [CrossRef]
14. Huang, H.; Wang, J.; Zhang, J.; Cai, J.; Pi, J.; Xu, J.-F. Inspirations of Cobalt Oxide Nanoparticle Based Anticancer Therapeutics. *Pharmaceutics* **2021**, *13*, 1599. [CrossRef] [PubMed]
15. Parveen, K.; Banse, V.; Ledwani, L. Green synthesis of nanoparticles: Their advantages and disadvantages. In *Proceedings of the AIP Conference Proceedings*; AIP Publishing LLC: Melville, NY, USA, 2016; Volume 1724, p. 020048. [CrossRef]
16. Thema, F.; Manikandan, E.; Dhlamini, M.; Maaza, M. Green synthesis of ZnO nanoparticles via Agathosma betulina natural extract. *Mater. Lett.* **2015**, *161*, 124–127. [CrossRef]
17. Manikandan, V.; Jayanthi, P.; Priyadharsan, A.; Vijayaprathap, E.; Anbarasan, P.M.; Velmurugan, P. Green synthesis of pH-responsive Al_2O_3 nanoparticles: Application to rapid removal of nitrate ions with enhanced antibacterial activity. *J. Photochem. Photobiol. A Chem.* **2019**, *371*, 205–215. [CrossRef]
18. Fadus, M.C.; Lau, C.; Bikhchandani, J.; Lynch, H.T. Curcumin: An age-old anti-inflammatory and anti-neoplastic agent. *J. Tradit. Complement. Med.* **2016**, *7*, 339–346. [CrossRef]
19. Alsamydai, A.; Jaber, N. Pharmacological aspects of curcumin. *Int. J. Pharm.* **2018**, *5*, 313–326.
20. Fouda, A.; Al-Otaibi, W.A.; Saber, T.; AlMotwaa, S.M.; Alshallash, K.S.; Elhady, M.; Badr, N.F.; Abdel-Rahman, M.A. Antimicrobial, antiviral, and in-vitro cytotoxicity and mosquitocidal activities of Portulaca oleracea-based green synthesis of selenium nanoparticles. *J. Funct. Biomater.* **2018**, *13*, 157. [CrossRef] [PubMed]
21. Fouda, A.; Hassan SE, D.; Eid, A.M.; Awad, M.A.; Althumayri, K.; Badr, N.F.; Hamza, M.F. Endophytic bacterial strain, Brevibacillus brevis-mediated green synthesis of copper oxide nanoparticles, characterization, antifungal, in vitro cytotoxicity, and larvicidal activity. *Green Process. Synth.* **2022**, *11*, 931–950. [CrossRef]
22. Fouda, A.; Eid, A.M.; Guibal, E.; Hamza, M.F.; Hassan SE, D.; Alkhalifah DH, M.; El-Hossary, D. Green Synthesis of Gold Nanoparticles by Aqueous Extract of Zingiber officinale: Characterization and Insight into Antimicrobial, Antioxidant, and In Vitro Cytotoxic Activities. *Appl. Sci.* **2022**, *12*, 12879. [CrossRef]
23. Fouda, A.; Awad, M.A.; Eid, A.M.; Saied, E.; Barghoth, M.G.; Hamza, M.F.; Awad, M.F.; Abdelbary, S.; Hassan, S.E.D. An Eco-friendly approach to the control of pathogenic microbes and anopheles stephensi malarial vector using Magnesium Oxide Nanoparticles (Mg-NPs) fabricated by Penicillium chrysogenum. *Int. J. Mol. Sci.* **2021**, *22*, 5096. [CrossRef]
24. Fouda, A.; Eid, A.M.; Abdel-Rahman, M.A.; El-Belely, E.F.; Awad, M.A.; Hassan, S.E.D.; Al-Faifi, Z.E.; Hamza, M.F. Enhanced Antimicrobial, Cytotoxicity, Larvicidal, and Repellence Activities of Brown Algae, Cystoseira crinita-Mediated Green Synthesis of Magnesium Oxide Nanoparticles. *Front. Bioeng. Biotechnol.* **2022**, *10*, 849921. [CrossRef]
25. Parvathiraja, C.; Shailajha, S.; Shanavas, S.; Gurung, J. Biosynthesis of silver nanoparticles by Cyperus pangorei and its potential in structural, optical and catalytic dye degradation. *Appl. Nanosci.* **2020**, *11*, 477–491. [CrossRef]
26. Parvathiraja, C.; Shailajha, S. Bioproduction of CuO and Ag/CuO heterogeneous photocatalysis-photocatalytic dye degradation and biological activities. *Appl. Nanosci.* **2021**, *11*, 1411–1425. [CrossRef]
27. Fouda, A.; Eid, A.M.; Abdelkareem, A.; Said, H.A.; El-Belely, E.F.; Alkhalifah, D.H.M.; Alshallash, K.S.; Hassan, S.E.-D. Phyco-Synthesized Zinc Oxide Nanoparticles Using Marine Macroalgae, *Ulva fasciata* Delile, Characterization, Antibacterial Activity, Photocatalysis, and Tanning Wastewater Treatment. *Catalysts* **2022**, *12*, 756. [CrossRef]
28. Pallavolu, M.R.; Krishna, K.G.; Nagaraju, G.; Babu, P.S.; Sambasivam, S.; Sreedhar, A. Rational design of Cu-doped Co_3O_4@carbon nanocomposite and agriculture crop-waste derived activated carbon for high-performance hybrid supercapacitors. *J. Ind. Eng. Chem.* **2022**, *116*, 428–437. [CrossRef]
29. Kéranguéven, G.; Filimonenkov, I.S.; Savinova, E.R. Investigation of the stability of the boron-doped diamond support for Co_3O_4-based oxygen evolution reaction catalysts synthesized through in situ autocombustion method. *J. Electroanal. Chem.* **2022**, *916*, 116367. [CrossRef]
30. Yang, H.; Zhang, D.; Luo, Y.; Yang, W.; Zhan, X.; Yang, W.; Hou, H. Highly Efficient and Selective Visible-Light Driven Photoreduction of CO_2 to CO by Metal–Organic Frameworks-Derived Ni—Co—O Porous Microrods. *Small* **2022**, *18*, 2202939. [CrossRef]
31. Bahadoran, A.; Ramakrishna, S.; Oryani, B.; Al-Keridis, L.A.; Nodeh, H.R.; Rezania, S. Biodiesel production from waste cooking oil using heterogeneous nanocatalyst-based magnetic polyaniline decorated with cobalt oxide. *Fuel* **2022**, *319*, 123858. [CrossRef]
32. Tang, C.-W.; Wang, C.-B.; Chien, S.-H. Characterization of cobalt oxides studied by FT-IR, Raman, TPR and TG-MS. *Thermochim. Acta* **2008**, *473*, 68–73. [CrossRef]
33. Puspalak, A.; Chinnadurai, P.; Prathibha, R.; Kumar, M.P.; Manjushree, S.G.; UdayaKumar, V.; Adarakatti, P.S. Cobalt oxide nanoparticles based carbon electrode for the detection of residual nitrite in the soil of agricultural fields. *Mater. Res. Innov.* **2022**, *27*, 100–109. [CrossRef]

34. Asha, G.; Rajeshwari, V.; Stephen, G.; Gurusamy, S.; Rachel, D.C.J. Eco-friendly synthesis and characterization of cobalt oxide nanoparticles by sativum species and its photo-catalytic activity. *Mater. Today: Proc.* **2021**, *48*, 486–493. [CrossRef]
35. Reena, R.S.; Aslinjensipriya, A.; Infantiya, S.G.; Britto JD, J.; Jose, M.; Das, S.J. Visible-light active zinc doped cobalt oxide (Zn-Co_3O_4) nanoparticles for photocatalytic and photochemical activity. *Mater. Today Proc.* **2022**, *68*, 269–275. [CrossRef]
36. Gopinath, S.; Mayakannan, M.; Vetrivel, S. Structural, optical, morphological properties of silver doped cobalt oxide nanoparticles by microwave irradiation method. *Ceram. Int.* **2021**, *48*, 6103–6115. [CrossRef]
37. Maharani, N.Y. Structural, morphological, optical properties of Zr-doped Co_3O_4 nanoparticles. *Part. Sci. Technol.* **2022**, *40*, 662–674.
38. Feng, Z.; Zhu, X.; Yang, J.; Zhong, K.; Jiang, Z.; Yu, Q.; Song, Y.; Hua, Y.; Li, H.; Xu, H. Inherent Facet-Dominant effect for cobalt oxide nanosheets to enhance photocatalytic CO_2 reduction. *Appl. Surf. Sci.* **2022**, *578*, 151848. [CrossRef]
39. Gouasmia, A.; Zouaoui, E.; Mekkaoui, A.A.; Haddad, A.; Bousba, D. Highly efficient photocatalytic degradation of malachite green dye over copper oxide and copper cobaltite photocatalysts under solar or microwave irradiation. *Inorg. Chem. Commun.* **2022**, *145*, 110066. [CrossRef]
40. Gopinath, S.; Mayakannan, M.; Vetrivel, S. Analysis on the effect of doping in structural, morphological, and antibacterial properties of Yttrium doped cobalt oxide nanoparticles. *Mater. Technol.* **2022**, *37*, 2425–2435. [CrossRef]
41. Samer, M.; Abdelsalam, E.M.; Mohamed, S.; Elsayed, H.; Attia, Y. Impact of photoactivated cobalt oxide nanoparticles addition on manure and whey for biogas production through dry anaerobic co-digestion. *Environ. Dev. Sustain.* **2021**, *24*, 7776–7793. [CrossRef]
42. Haase, F.T.; Bergmann, A.; Jones, T.E.; Timoshenko, J.; Herzog, A.; Jeon, H.S.; Rettenmaier, C.; Cuenya, B.R. Size effects and active state formation of cobalt oxide nanoparticles during the oxygen evolution reaction. *Nat. Energy* **2022**, *7*, 765–773. [CrossRef]
43. Natarajan, K. Photodegradation studies of pure and cobalt doped zinc oxide nanoparticles. *Mater. Res. Innov.* **2022**, *27*, 69–74. [CrossRef]
44. Singh, A.K. A review on plant extract-based route for synthesis of cobalt nanoparticles: Photocatalytic, electrochemical sensing and antibacterial applications. *Curr. Res. Green Sustain. Chem.* **2022**, *5*, 100270. [CrossRef]
45. Rathika, G.; Suba, V.; Lakshmi, D.S.; Rani, R. Exploring the Biosynthesized Metal Nanoparticles for their Catalytic Degradation of Toxic Water Wastes and Antimicrobial Potential. *J. Inorg. Organomet. Polym. Mater.* **2022**, *32*, 3153–3169. [CrossRef]
46. Alagumalai, K.; Shanmugam, R.; Chen, T.W.; Chen, S.M.; Balamurugan, M.; Choi, S.S.; Ali, M.A.; Al-Mohaimeed, A.M.; Fan, C.H. The electrochemical evaluation of antipsychotic drug (promethazine) in biological and environmental samples through samarium cobalt oxide nanoparticles. *Mater. Today Chem.* **2022**, *25*, 100961. [CrossRef]
47. Tien, T.M.; Chen, C.H.; Huang, C.T.; Chen, E.L. Photocatalytic Degradation of Methyl Orange Dyes Using Green Synthesized MoS2/Co_3O_4 Nanohybrids. *Catalysts* **2022**, *12*, 1474. [CrossRef]
48. Vinayagam, R.; Hebbar, A.; Kumar, P.S.; Rangasamy, G.; Varadavenkatesan, T.; Murugesan, G.; Srivastava, S.; Goveas, L.C.; Kumar, N.M.; Selvaraj, R. Green synthesized cobalt oxide nanoparticles with photocatalytic activity towards dye removal from water environment. *Environ. Res.* **2022**, *216*, 114766. [CrossRef] [PubMed]
49. Kurniawan, T.A.; Mengting, Z.; Fu, D.; Yeap, S.K.; Othman, M.H.D.; Avtar, R.; Ouyang, T. Functionalizing TiO2 with graphene oxide for enhancing photocatalytic degradation of methylene blue (MB) in contaminated wastewater. *J. Environ. Manag.* **2020**, *270*, 110871. [CrossRef] [PubMed]
50. Zhang, J.; Tian, B.; Wang, L.; Xing, M.; Lei, J. *Photocatalysis*; Springer: Singapore, 2018; pp. 1–15. [CrossRef]
51. Tomar, R.; Abdala, A.A.; Chaudhary, R.G.; Singh, N. Photocatalytic degradation of dyes by nanomaterials. *Mater. Today Proc.* **2020**, *29*, 967–973. [CrossRef]
52. Vennela, A.B.; Mangalaraj, D.; Muthukumarasamy, N.; Agilan, S.; Hemalatha, K.V. Structural and optical properties of Co_3O_4 nanoparticles prepared by sol-gel technique for photocatalytic application. *Int. J. Electrochem. Sci.* **2019**, *14*, 3535–3552. [CrossRef]
53. Chowdhury, B.; Pradhan, S.S.; Das, H.S.; Biswas, B. Visible Light Induced Photocatalytic Dye Degradation by Cobalt Oxide Nanoparticles. *Fine Chem. Eng.* **2020**, *1*, 104–117. [CrossRef]
54. Bibi, I.; Nazar, N.; Iqbal, M.; Kamal, S.; Nawaz, H.; Nouren, S.; Safa, Y.; Jilani, K.; Sultan, M.; Ata, S.; et al. Green and eco-friendly synthesis of cobalt-oxide nanoparticle: Characterization and photo-catalytic activity. *Adv. Powder Technol.* **2017**, *28*, 2035–2043. [CrossRef]
55. Saravan, R.S.; Muthukumaran, M.; Mubashera, S.M.; Abinaya, M.; Prasath, P.V.; Parthiban, R.; Mohammad, F.; Oh, W.C.; Sagadevan, S. Evaluation of the photocatalytic efficiency of cobalt oxide nanoparticles towards the degradation of crystal violet and methylene violet dyes. *Optik* **2020**, *207*, 164428. [CrossRef]
56. Verma, M.; Mitan, M.; Kim, H.; Vaya, D. Efficient photocatalytic degradation of Malachite green dye using facilely synthesized cobalt oxide nanomaterials using citric acid and oleic acid. *J. Phys. Chem. Solids* **2021**, *155*, 110125. [CrossRef]
57. Yousefi, S.R.; Alshamsi, H.A.; Amiri, O.; Salavati-Niasari, M. Synthesis, characterization and application of Co/Co_3O_4 nanocomposites as an effective photocatalyst for discoloration of organic dye contaminants in wastewater and antibacterial properties. *J. Mol. Liq.* **2021**, *337*, 116405. [CrossRef]
58. Adekunle, A.S.; Oyekunle, J.A.; Durosinmi, L.M.; Oluwafemi, O.S.; Olayanju, D.S.; Akinola, A.S.; Obisesan, O.R.; Akinyele, O.F.; Ajayeoba, T.A. Potential of cobalt and cobalt oxide nanoparticles as nanocatalyst towards dyes degradation in wastewater. *Nano-Struct. Nano-Objects* **2020**, *21*, 100405. [CrossRef]

59. Magdalane, C.M.; Kaviyarasu, K.; Arularasu, M.; Kanimozhi, K.; Ramalingam, G. Structural and morphological properties of Co_3O_4 nanostructures: Investigation of low temperature oxidation for photocatalytic application for waste water treatment. *Surf. Interfaces* **2019**, *17*, 100369. [CrossRef]
60. Dhiman, S.; Gupta, B. Co_3O_4 nanoparticles synthesized from waste Li-ion batteries as photocatalyst for degradation of methyl blue dye. *Environ. Technol. Innov.* **2021**, *23*, 101765. [CrossRef]
61. Siddique, M.; Khan, N.M.; Saeed, M.; Ali, S.; Shah, Z. Green synthesis of cobalt oxide nanoparticles using *Citrus medica* leaves extract: Characterization and photo-catalytic activity. *Z. Für Phys. Chem.* **2020**, *235*, 663–681. [CrossRef]
62. Fouda, A.; Hassan SE, D.; Eid, A.M.; Abdel-Rahman, M.A.; Hamza, M.F. Light enhanced the antimicrobial, anticancer, and catalytic activities of selenium nanoparticles fabricated by endophytic fungal strain, Penicillium crustosum EP-1. *Sci. Rep.* **2022**, *12*, 11834. [CrossRef]
63. Fouda, A.; Awad, M.A.; Al-Faifi, Z.E.; Gad, M.E.; Al-Khalaf, A.A.; Yahya, R.; Hamza, M.F. Aspergillus flavus-Mediated Green Synthesis of Silver Nanoparticles and Evaluation of Their Antibacterial, Anti-Candida, Acaricides, and Photocatalytic Activities. *Catalysts* **2022**, *12*, 462. [CrossRef]
64. Fouda, A.; Hassan SE, D.; Saied, E.; Hamza, M.F. Photocatalytic degradation of real textile and tannery effluent using biosynthesized magnesium oxide nanoparticles (MgO-NPs), heavy metal adsorption, phytotoxicity, and antimicrobial activity. *J. Environ. Chem. Eng.* **2021**, *9*, 105346. [CrossRef]
65. Singh, J.; Singh, G.P.; Jain, R.K.; Singh, B.; Singh, K.J.; Singh, R.C. Effect of calcination temperature on structural, optical and antibacterial properties of ball mill synthesized Co_3O_4 nanomaterials. *J. Mater. Sci. Mater. Electron.* **2022**, *33*, 3250–3266. [CrossRef]
66. Anuradha, C.; Raji, P. Facile-synthesis and characterization of cobalt oxide (Co_3O_4) nanoparticles by using Arishta leaves assisted biological molecules and its antibacterial and antifungal activities. *J. Mol. Struct.* **2022**, *1262*, 133065. [CrossRef]

Disclaimer/Publisher's Note: The statements, opinions and data contained in all publications are solely those of the individual author(s) and contributor(s) and not of MDPI and/or the editor(s). MDPI and/or the editor(s) disclaim responsibility for any injury to people or property resulting from any ideas, methods, instructions or products referred to in the content.